



ELSEVIER

Available online at www.sciencedirect.com

SCIENCE @ DIRECT®

Journal of volcanology
and geothermal research

Journal of Volcanology and Geothermal Research 130 (2004) 93–105

www.elsevier.com/locate/jvolgeores

The nature and timing of caldera collapse as indicated by accidental lithic fragments from the AD ~1000 eruption of Volcán Ceboruco, Mexico

B.L. Browne*, J.E. Gardner

University of Alaska Fairbanks Geophysical Institute, 903 Koyukuk Drive, Fairbanks, AK 99775, USA

Received 7 October 2002; accepted 24 July 2003

Abstract

One way to determine the mechanics of caldera formation is through quantitative component analysis of accidental lithic fragments in pyroclastic deposits erupted before and during caldera collapse. All previous studies of this sort, however, are based on pyroclastic deposits from large-volume ($> 10 \text{ km}^3$) caldera eruptions. In this study, we use quantitative component analysis of lithic fragments to determine the mechanics of the AD ~1000 small-volume ($3\text{--}4 \text{ km}^3$ DRE) caldera eruption of Volcán Ceboruco, located in western Mexico. During this eruption, caldera collapse occurred in such a way that lithic fragments of decreasing depths were preferentially erupted with time. Prior to caldera collapse, deep-origin lithics ($\sim 6 \text{ km}$ depth) and vent-derived lithics were erupted. Deposits emplaced during collapse, however, contain a distinctly different population of lithic fragments, such as lithics from mid-depth origin ($\sim 1 \text{ km}$ depth) and from the vent. By the end of the eruption, the total amount of lithic material in the deposits had increased from $< 15 \text{ wt}\%$ before collapse to as much as $90 \text{ wt}\%$, yet this material contains essentially no lithics of deep origin. This suggests that collapse resulted in the obstruction of both deep-origin lithics and magma from reaching the surface. Based on these data, we suggest that collapse occurred as a result of the fracturing and subsequent failure of the overlying magma reservoir roof that occurred along inward dipping faults. The collapse forced the fragmentation depth and progressive erosion of lithic material from deep to shallow depths, which subsequently sealed the conduit, stopping the eruption.

© 2003 Elsevier B.V. All rights reserved.

Keywords: caldera eruptions; caldera collapse; accidental lithics; Volcán Ceboruco; Marquesado pyroclastic flow

1. Introduction

Caldera-forming volcanic eruptions, which may erupt up to 5000 km^3 of magma, are catastrophic

events that pose one of the greatest natural hazards on Earth (Smith, 1979; Lipman, 1984). Even relatively small caldera eruptions may result in several thousand deaths and alter global climate (Rampino and Self, 1982; Newhall and Punongbayan, 1996). The mechanics of caldera formation in volcanic eruptions, however, remain poorly understood as a result of the infrequency of such eruptions and the extreme difficulty in ob-

* Corresponding author. Tel: 1-907-474-1925; fax: 1-907-474-5361.

E-mail address: ftblb@uaf.edu (B.L. Browne).

servicing them. Determining how caldera collapse occurs will lead to a more comprehensive understanding of volcanic processes, resulting in more accurate and realistic hazard assessment.

The general process of caldera collapse is thought to be the same regardless of total erupted volume, such that enough magma erupts to cause the volcano to collapse (Williams, 1941; Smith and Bailey, 1968). Studies of pyroclastic deposits from caldera eruptions, however, indicate that differences exist as a function of the total volume of erupted material. Large volume ($> 10 \text{ km}^3$) caldera-forming eruption deposits of, for example, Crater Lake and Long Valley suggest that collapse began after a relatively small volume of magma was erupted, and that the volume of magma erupted during collapse overwhelmingly dominates the volume of magma erupted prior to collapse (Hildreth, 1977; Bacon, 1983; Suzuki-Kamata et al., 1993; Wilson and Hildreth, 1997). Studies of deposits from smaller volume ($< 5 \text{ km}^3$) caldera eruptions, for example, the AD 79 eruption of Vesuvius and the 1991 eruption of Pinatubo, on the other hand, indicate that collapse occurred after the majority of magma was erupted, and that the total collapsed volume equals the total volume of erupted magma – not just that ejected during collapse (Sigurdsson et al., 1985; Carey and Sigurdsson, 1987; Scott et al., 1996; Gardner and Tait, 2000). The difference between small- and large-volume caldera eruptions may be related to the mechanics of collapse itself.

In order to investigate the differences in collapse between small and large calderas, we undertook a quantitative component analysis of the eruptive stratigraphy from the AD ~ 1000 caldera-forming eruption of Volcán Ceboruco, located in western Mexico. Lithic fragments in pyroclastic deposits result from conduit and vent erosion during explosive eruptions, and so they can record changes in the mechanics of collapse and the timing of collapse onset (Heiken and McCoy, 1984; Hildreth, 1991; Suzuki-Kamata et al., 1993; Wilson and Hildreth, 1997). Previous studies (see above) have only focused on large calderas, and so our work augments those studies by focusing on a small-volume caldera.

2. Geologic setting

Volcán Ceboruco, a 2164-m-high composite volcano, is one of the westernmost active volcanoes in the Trans-Mexican Volcanic Belt (Gunn and Mooser, 1971) (Fig. 1). The summit is truncated by two concentric calderas, the older of which measures $\sim 4 \text{ km}$ in diameter while the younger is $\sim 1.5 \text{ km}$ in diameter (Nelson, 1980; Gardner and Tait, 2000). Ceboruco is situated in a $\text{N}60^\circ\text{W}$ -trending graben structure that comprises the Jala and Ahuacatlán valleys. A prominent escarpment composed of the Jala–Juanacata Group, composed of Pliocene-aged rhyolitic ash-flow tuffs, abruptly marks the northern margin of this graben (Ferrari et al., 2000). These cliffs rise in excess of 230 m above the valley floor and represent the front of a rugged plateau that extends to the north. Many workers speculate that this escarpment is suggestive of a normal fault scarp (Thorpe and Francis, 1975; Demant, 1978; Ferrari et al., 2000), however Nelson (1980) concluded that not enough direct evidence exists to accurately determine subsidence rates. Gunn and Mooser (1971) and Nelson (1980) proposed that Juan–Juanacata tuff likely exists immediately beneath Ceboruco. The concealed deeper levels beneath Ceboruco are composed in part of granitic material, because such xenoliths are often found in the erupted products from cinder cones located immediately adjacent to the northwest and southeast of Ceboruco (Thorpe and Francis, 1975; Nelson, 1980), and in several different erupted deposits of Volcán Ceboruco (Nelson, 1980; Browne, 2001).

The edifice of Ceboruco is composed predominantly of andesitic lava flows (Nelson, 1980). Two silicic domes exist on the eastern flanks near Jala, and several monogenetic cinder cones exist in a $\sim \text{N}50^\circ\text{W}$ -trending chain to the SE and NW of Ceboruco (Fig. 1). The AD ~ 1000 eruption (^{14}C ages from charcoal samples collected by Nelson (1980) from beneath the Jala Pumice and in the middle of the Marquesado pyroclastic flows yield ages of 1010 ± 200 , 1030 ± 200 and $1500 \pm 300 \text{ BP}$) resulted in the deposition of $3\text{--}4 \text{ km}^3$ (DRE) of magma as the Jala Pumice deposit to the north and northeast and the Marquesado

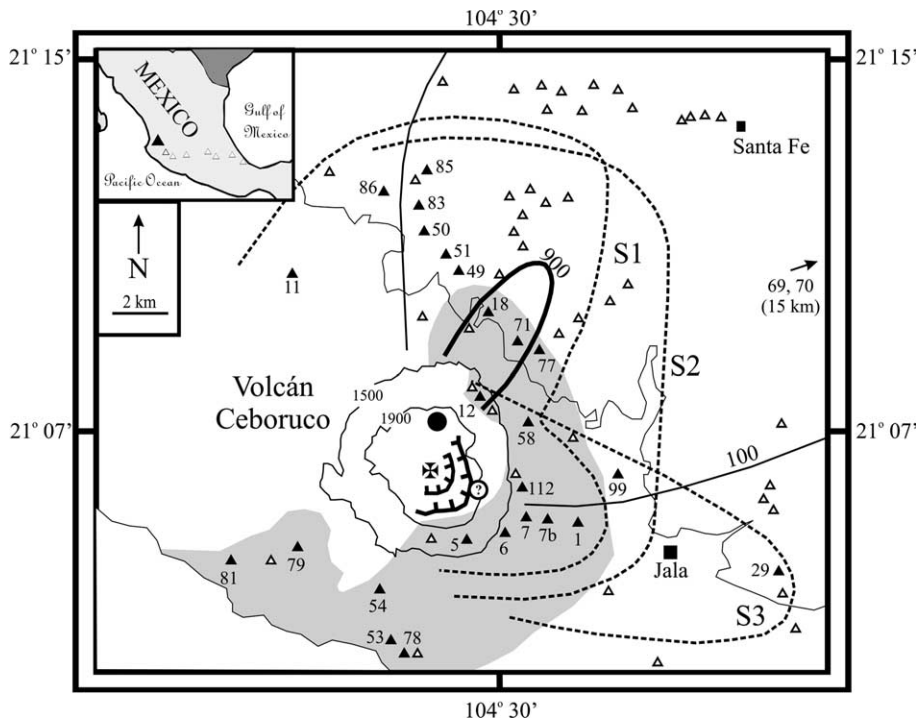


Fig. 1. Sample locality and isopach map for the different layers of the Jala Pumice with the north-flank vent (circle) and two calderas noted. 1-cm isopachs for S1, S2, and S3 pyroclastic surge deposits (dashed); and 5-cm isopachs for the Marquesado and North-Flank PFDs (shaded) are indicated. In addition, both the >100 - and >900 -cm isopachs for the Plinian fall deposits (thin and bold lines, respectively), and the location of the north-flank vent (shaded circle) are provided (from Gardner and Tait, 2000). Plateaus to the north and south of Ceboruco are composed of Pliocene-aged Jala–Juanacata unit. Solid triangles indicate sample localities where component analysis of the deposits was performed for this study, whereas open triangles indicate other localities used for isopach correlation. Sample locality numbers are specifically noted adjacent to their respective locations (see text). Inset map shows location of Volcán Ceboruco in the Trans-Mexican Volcanic Belt. Azimuth measurements of pyroclastic deposits from specific localities are measured from center of caldera, marked with errors.

pyroclastic flow deposits (PFDs) to the south, along with the formation of the outer caldera, which remains open to the south (Nelson, 1980; Gardner and Tait, 2000). The most obvious evidence that the AD ~ 1000 eruption resulted in the formation of the outer caldera is the truncated, nearly flat, summit of Ceboruco that is partially enclosed by an outer wall that rises approximately 100 m above the nearly flat floor. Jala Pumice deposits are also found within and atop the outer caldera walls, but not within the inner caldera, indicating that the AD ~ 1000 eruption was the last eruption prior to the collapse of the outer caldera. On the western and southwestern sides of Ceboruco, the walls are covered by subsequently emplaced lava flows, but even these flows lie at an elevation of more than 100 m below the

flat caldera floor. Nelson (1980) argued that this evidence required that the caldera was at least 200 m deep at the time of its formation. Assuming that the pre-caldera Ceboruco was relatively flat topped, that the caldera was circular (~ 4 km in diameter) and that collapse was on the average 250 m, the collapse volume of the outer caldera would equal 3.1 km^3 . If, on the other hand, we were to imagine that the pre-caldera Ceboruco was conical and project the slope of the flanks upward, it is estimated that Ceboruco would have attained an elevation of 2700 m, or 500 m above its present caldera wall. Assuming that the collapse was on the average 250 m, this calculation also results in a volume of 3.1 km^3 . These approximations are comparable to the volume estimate for the erupted magma volume of the Jala

Pumice of 3–4 km³ that was calculated by Gardner and Tait (2000).

Following the AD ~1000 eruption, the Dos Equis dacite lava dome was emplaced, partially filling the caldera. Continued lava extrusions, ranging from basaltic andesite to dacite in composition, destabilized this dome, causing it to collapse and form a smaller caldera that is nested inside the outer caldera (Nelson, 1980). Because the Jala Pumice deposit is found only on the outer flanks of Ceboruco and atop the outer caldera walls, but is nowhere observed within the inside caldera, it could not have been associated with the second caldera eruption. Historical activity of Ceboruco is limited to an eruption in 1870–1872, where a dacite lava flow and pyroclastic deposits were emplaced on the western flanks of the cone (Ordoñez, 1897). Weak fumarolic activity from this eruption persists today.

3. Overview of the AD ~1000 caldera-forming eruption

Gardner and Tait (2000) and Browne (2001)

studied the climactic eruption of Volcán Ceboruco, and their findings are summarized here. The AD ~1000 eruption deposited approximately 3–4 km³ (DRE) of rhyodacitic and dacitic pumice known as the Jala Pumice (including the Marquesado PFDs), resulting in a 3.7-km-diameter caldera. The Jala Pumice consists of a thick sequence of alternating pumice fall and ash layers that extend mostly to the northeast, whereas the Marquesado deposits are found primarily on the eastern flanks and to the southwest (Fig. 1).

Phase I of the eruption was characterized by the establishment of a Plinian column, where a thin, lithic-rich fall layer (P0) was narrowly distributed to the north. Next, the most voluminous and widely dispersed Plinian fall deposit (P1) was deposited to the northeast. Both of the Phase I deposits were erupted from a vent on the north flank (Fig. 1), as indicated by the isopach maps generated by Gardner and Tait (2000). During most of the eruption of Phase I, eruptive intensity (mass flux) gradually increased from 4×10^7 to 8×10^7 kg/s, producing a Plinian column 25–30 km in height. Abrupt normal grading at the top of P1 indicates, however, that mass flux waned

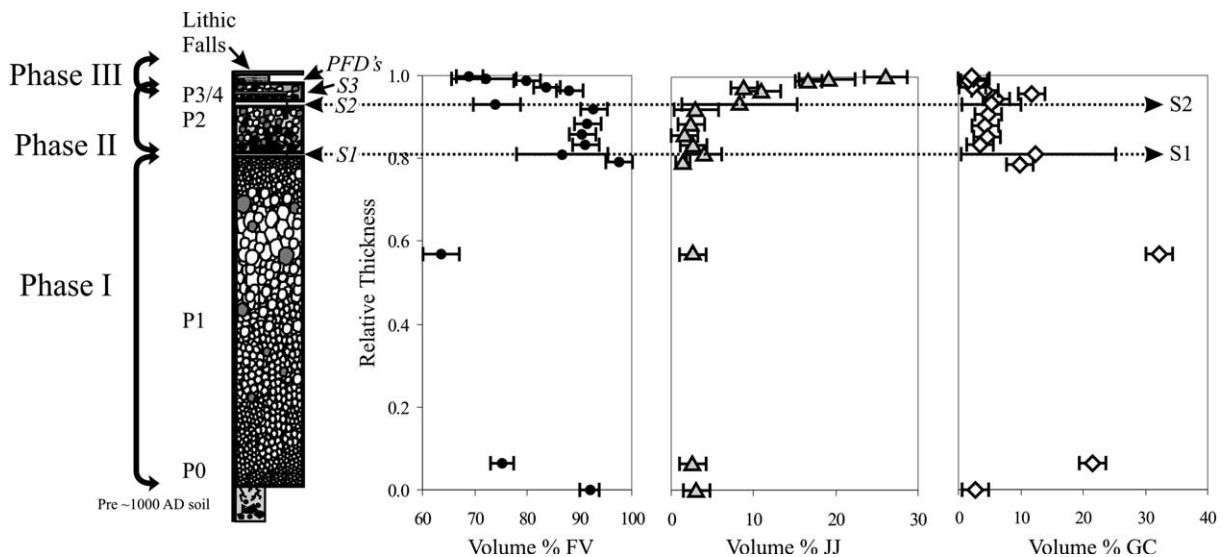


Fig. 2. Stratigraphic section through the Jala Pumice at Locality 18 (see Fig. 1). The relative size and proportions of lithics (solid), and white, gray, and banded pumice are schematically indicated in the section (left). Abundance of Fresh Volcanic (FV, circles), Jala-Juanacata (JJ, triangles), and Granitic Clast (GC, diamonds) lithics are plotted with stratigraphic height, with S1 and S2 proportions indicated for added clarity. Data points signify the average vol% for each lithic type, with the range of vol% from all samples represented by the error bars. For the number of analyzed samples per data point, refer to Table 1.

rapidly, and possibly that there was a brief pause in the eruption.

Phase II of the eruption began similarly to Phase I, with the eruption of a thin, narrowly deposited, lithic-rich layer immediately atop P1 of equal volume and dispersal direction as P0. Subsequent Phase II activity is characterized by a transitional regime, feeding both a Plinian column and dilute density currents. During Phases II and III of the eruption, a much smaller volume of magma was erupted as alternating Plinian fall and pyroclastic surges. Mass flux varied by more than an order of magnitude in Phase II, resulting in significant fluctuations in lithic content, magma composition, grading, and eruptive style (Fig. 2). Isopach maps of Plinian fall deposits (P2, P3/4) indicate that they were erupted from the north-flank vent only and were dispersed to the northeast. In contrast, pyroclastic surge isopachs display a progressive change in dispersal direction with subsequently emplaced surge deposits in a clockwise direction from the north to the southwest (Browne, 2001). Isopachs corresponding to the first surge deposit (S1) are in two lobes, one extending north and one extending east. Isopachs of the second surge deposit (S2) broadly exist to the northeast, and isopachs from the third surge deposit (S3) extend in a narrow lobe to the east. There is no direct exposure of an eruptive vent on the southeastern flanks, but we can infer its location from the progressive shift in distribution of pyroclastic surge deposit isopachs (Fig. 1).

Gardner and Tait (2000) argued that the onset of caldera collapse occurred at the beginning of Phase II with the following evidence. Large variations in size and grading of lithics exist in Phase II fall deposits (P2, P3, and P4) compared with P1, suggesting that the mass flux of the eruptive column depositing them was highly variable, and thus unstable, compared with that of P1. Also, there are substantially more lithics in P2 (and subsequently erupted falls) than in P1, meaning that the proportion of lithics relative to magma in the erupting mixture was much higher during the deposition of P2.

The final phase of the eruption (Phase III) is characterized by an almost fully collapsing column, producing mostly dense pyroclastic flows

(Marquesado and North-Flank PFDs), fall (P5, P6) and lithic-fall deposits (L1, L2, and L3) (Fig. 2). Isopach mapping performed by Gardner and Tait (2000) indicates that P5 and P6 were dispersed along the same dispersal axis as all other Plinian fall deposits and originate from the north-flank vent. At least two Marquesado pyroclastic flow deposit layers of equivalent thickness, color, and internal stratigraphy persist from the southern flank to the eastern flank where they are stratigraphically equivalent to the North-Flank PFDs (Browne, 2001). Isopach maps of the Phase III PFDs suggest that they were predominantly erupted to the north and south, whereas the Phase III lithic-fall deposits have only been found within 5 km to the southeast and east.

4. Methods

4.1. Field methods

The Jala Pumice tephra sequence was sampled at 27 sites (in all 84 samples) extending from the northwest to the southeast of Ceboruco (Fig. 1; Table 1). Plinian fall layers (P0, P1, P2, P3/4, and P5/6) were sampled at sites located 3–25 km along the main dispersal axis. P1 and P2 were sampled at several horizons within each deposit (e.g. base, middle, and top) for greater detail. Pyroclastic surge layers (S1, S2, S3) were sampled at sites surrounding the caldera rim. PFDs (Marquesado and North-Flank) were sampled along the rim, flanks, and adjacent valleys to the north, east, and south of the caldera rim.

4.2. Component analysis and description of lithic fragments

All samples were wet sieved at 0.5 ϕ intervals from -5.0ϕ to 4.5 ϕ . At least 1000 lithic fragments were counted from each sample collected (fall, surge, and flow deposits) from the 0.0 to 3.0 ϕ size ranges (1–0.125 mm). We divided the different types of lithic clasts into three main categories (fresh volcanics, FV; granitic clasts, GC; and Jala–Juanacata, JJ) and analyzed their proportions with respect to stratigraphic abundance

Table 1

Location, Jala Pumice horizon, sample number, azimuth, total lithic content, and the individual abundances of FV, GC, and JJ lithics based on the total number of counted lithic fragments

Locality	Horizon	Sample	Azimuth	Total Lithic Content (wt%)	FV (vol%)	GC (vol%)	JJ (vol%)	Total count
18	P0	P0-18	017	27.36	92.9	5.3	1.8	1109
50	P1 base	P1-50-0–15 cm	356	7.20	96.8	1.4	1.8	1548
1	P1 base	P1-01-0–20 cm	015	9.14	98.5	1.5	0.0	1682
18	P1 base	P1-18-0–70 cm	017	5.84	98.1	1.8	0.1	1154
29	P1 base	P1-29-0–20 cm	105	10.05	97.6	2.1	0.3	1139
69	P1 base	P1-69-0–30 cm	077	6.36	98.5	1.4	0.1	1368
69	P1 middle	P1-69-57–87 cm	077					
1	P1 middle	P1-01-120–135 cm	104	7.55	83.1	16.9	0.0	1275
18	P1 middle	P1-18-200–220 cm	017	9.07	72.8	25.8	1.4	1982
18	P1 middle	P1-18-550–560 cm	017	14.56	74.4	24.6	1.0	2361
29	P1 middle	P1-29-120–140 cm	105	3.80	75.6	22.8	1.6	1579
1	P1 top	P1-01-227–247 cm	015	14.69	96.8	1.9	1.3	1556
18	P1 top	P1-18-(–20–40) cm	017	8.23	98.5	1.5	0.0	1770
18	P1 top	P1-18-(–20) cm	017	17.55	98.6	1.4	0.0	1797
29	P1 top	P1-29-(–15) cm	105	9.67	97.8	1.8	0.4	1874
50	P1 top	P1-50-(–15) cm	356	17.21	96.7	1.9	1.4	1205
69	P1 top	P1-69-(–10) cm	077	11.28	96.8	2.1	1.1	1952
18	P1 f.g.t.	P1-18-upper cm	017	45.30	86.1	13.5	0.4	2102
11	S1	CBV-11-1	318	45.05	77.6	22.4	0.0	1918
86	S1	CBV-S-17	346	50.78	91.6	8.2	0.2	16.39
83	S1	CBV-S-13	353	28.13	94.0	6.0	0.0	1059
50	S1	CBV-S-11	356	39.74	95.8	3.9	0.4	1113
49	S1	CBV-S-6	004	49.42	92.1	5.1	2.8	1721
18	S1	CBV-S-1	017	40.01	92.0	5.4	2.7	2225
12	S1	CBV-12-1	022	56.64	94.6	3.4	2.0	3490
71	S1	CBV-S-25	030	45.59	91.5	6.1	2.4	1874
77	S1	CBV-S-29	041	59.03	97.2	1.0	1.8	2231
6	S1	CBV-6-1	117	26.28	94.9	3.4	1.7	1558
5	S1	CBV-5-1	131	25.66	94.0	1.3	4.7	1893
50	P2 base	P2-50-0–20 cm	356	75.43	89.6	5.9	4.5	1128
1	P2 base	P2-01-0–20 cm	104	51.68	91.5	4.8	3.7	1098
18	P2 base	P2-18-0–26 cm	017	58.70	92.1	5.3	2.6	1039
70	P2 base	P2-70-0–10 cm	077	23.60	92.9	5.4	1.7	1238
29	P2 base	P2-29-0–10 cm	105	36.78	93.8	5.1	1.1	1401
18	P2 lower	P2-18-26–66 cm	017	28.17	89.0	8.2	2.8	1530
70	P2 lower	P2-70-CPL	077	14.20	84.8	12.9	2.3	1894
18	P2 upper	P2-18-83–111 cm	017	40.21	91.3	6.6	2.1	2174
18	P2 top	P2-18-111–118 cm	017	48.96	94.3	5.4	0.3	2609
70	P2 top	P2-70-top	077	32.59	95.8	3.7	0.5	2141
85	S2	CBV-S-29	357	28.15	71.9	28.1	0.0	1529
51	S2	CBV-S-1	000	29.12	72.1	27.9	0.0	1537
18	S2	CBV-S-6	017	23.23	86.3	10.5	3.1	2174
12	S2	CBV-12-6	022	34.33	84.7	7.3	8.0	1761
71	S2	CBV-12-1	030	31.50	90.3	1.9	7.8	2154
77	S2	CBV-S-28	041	29.41	86.6	2.7	10.7	1586
99	S2	CBV-6-1	107	47.21	84.8	3.9	11.4	1426
1	S2	CBV-1-1	104	40.30	86.7	4.1	9.2	1919
7	S2	CBV-S-11	108	55.62	83.9	3.4	12.7	1577
6	S2	CBV-6-4	117	24.64	81.7	5.2	13.1	1617
5	S2	CBV-S-13	131	67.74	88.0	0.0	12.0	1688
18	P3 base	P3/4-18-1	017	38.04	91.1	3.4	5.5	1687

Table 1 (Continued).

Locality	Horizon	Sample	Azimuth	Total Lithic Content (wt%)	FV (vol%)	GC (vol%)	JJ (vol%)	Total count
18	P3 top	P3/4-18-2	017	26.45	88.0	6.3	5.7	1625
12	S3	CBV-12-7b	022	67.13	86.0	6.1	7.9	2043
1	S3	BV-1-2	104	34.25	90.7	2.1	7.2	1627
99	S3	CBV-S-13	107	65.86	87.8	4.7	7.5	2308
6	S3	CBV-6-2	117	42.52	84.5	4.3	11.2	1597
18	P4 base	P3/4-18-3	017	30.44	90.4	3.4	6.2	1444
18	P4 top	P3/4-18-4	017	58.79	84.9	5.6	9.4	1778
12	F2	CBV-12-3	022	65.32	89.4	5.0	5.7	2330
12	F3 PL	CBV-12-4	022	87.64	82.0	9.2	8.7	2795
12	F3	CBV-12-5	022	76.42	88.0	2.1	9.8	2283
12	F4	CBV-12-8	022	51.93	86.3	2.4	11.3	2401
18	F?	CBV-S-3	017	31.10	88.2	1.7	10.1	1140
77	F?	CBV-F-2	041	61.83	93.1	1.0	5.9	2042
29	F?	CBV-29-2	274	29.40	81.5	9.2	9.2	2481
52	BASE	CBV-52-2a	192	60.20	88.6	2.0	9.4	2624
53	M1 LB	CBV-M-1	227	56.66	94.4	0.1	5.6	3311
79	M1 LB	CBV-M-6	256	65.54	95.3	0.0	4.7	4027
81	M1 BASE	CBV-M-13	211	78.36	94.8	0.0	5.2	3781
78	M1 PL	CBV-M-4	217	41.11	85.0	2.3	12.7	2495
53	M2	CBV-M-2	227	72.13	91.9	0.4	7.7	3423
79	M2 LB	CBV-M-8	256	68.83	95.7	0.0	4.3	3781
81	M2 MIDDLE	CBV-M-14	211	81.83	89.4	0.0	10.6	2756
53	M3	CBV-M-3	227	74.44	91.7	0.0	8.3	3881
54	M3 LB	CBV-M-5	224	84.95	90.4	0.0	9.6	2616
79	M3	CBV-M-9	256	54.42	92.1	0.0	7.9	3781
80	M3	CBV-M-10	253	30.23	87.3	0.0	12.7	1890
81	M3 TOP	CBV-M-16	211	32.82	95.2	0.0	4.8	1964
109	Lithic Fall 1	CBV-109-2	116	80.65	91.5	0.7	7.8	2639
112	Lithic Fall 1	CBV-112-1	105	92.90	81.1	0.5	18.4	2830
12	Lithic Fall 1	CBV-12e-3	022	67.28	87.5	0.1	12.4	2815
12	Lithic Fall 2	CBV-12e-2	022	86.71	84.7	0.7	14.6	3162
58	Lithic Fall 2	CBV-B-1a	079	65.77	93.3	0.0	6.7	2587
58	Lithic Fall 3	CBV-B-1c	079	76.24	84.6	1.8	13.6	2766

Plinian fall deposit sample numbers are indicative of the tephra layer, location number, and the height of the sampled horizon measured from either the base of the layer (i.e. 0–15 cm) or the top of the layer (i.e. –10 cm). Azimuth is measured from the center of the modern-day outer caldera rim (see Fig. 1).

(vol%) and location with respect to the caldera rim (azimuth) (Table 1). Little or no altered rock fragments were found (<0.5 vol%). The ranges in total lithic content as listed in this study are from the proximal deposits shown in Fig. 1 only, and therefore do not represent lithic contents for the deposit as a whole. Identification of lithic types was made with the aid of a hand lens and a binocular microscope.

Fresh volcanic rock types (FV) consist of crystal-poor basaltic andesite, pyroxene-bearing andesite, plagioclase-rich dacite, and minor obsidian

clasts. FV lithics are the most common lithic type found throughout the Jala Pumice, accounting for at least 60 vol% of lithics found in any given layer. All fresh volcanic rock types exist on the rim and flanks of Ceboruco as lava flows. Fresh volcanic rocks therefore are considered shallow-origin lithic fragments eroded from the uppermost levels of the conduit and vent.

Jala–Juanacata ignimbrite lithics (JJ) are pale olive green, and represent fragments from the Pliocene-aged rhyolite ash flow tuff that underlies Ceboruco and is found throughout western Mex-

ico (Ferrari et al., 2000). Mapping of the Jala–Juanacata unit in western Mexico by Ferrari et al. (1999) indicates that the average thickness of the unit near Ceboruco is ~ 300 m. The current rim of Ceboruco is approximately 1000 m above the graben floor, and so ~ 300 m of Jala–Juanacata is probably concealed beneath Ceboruco at a depth of at least 1000 m below the rim. JJ are thus considered to originate at mid-depth (~ 1 km depth) near the base of the conduit.

Granitic clasts (GC) are fine-to-medium-grained granodioritic fragments easily discerned from the other lithic types by their light color and unique mineralogy. Granitic clasts are composed of plagioclase, quartz, orthoclase \pm biotite, muscovite, and Fe–Ti oxides. Most of these clasts are partially melted, and probably formed wall rock of the AD ~ 1000 magma chamber.

5. Results

5.1. Phase I deposits

Lithic fragments found in the deposits from Phase I are consistent throughout the dispersal area. The P0 layer contains ~ 28 wt% total lithics, the majority of which is FV (92.9 vol%), with minor proportions of JJ (1.8 vol%) and GC (5.3 vol%) (Table 1; Fig. 2). P1 contains 5–15 wt% lithics. The base of P1 is dominated by FV (96.8–98.5 vol%) with few GC and JJ (1.4–2.1 vol% and < 1 –1.8 vol%, respectively). The middle and upper horizons of P1 contain greater amounts of GC (up to 25.9 vol%) with FV still accounting for the majority of lithic fragments (72.8–98.6 vol%). The abruptly fining horizon at the top of P1 contains ~ 45 wt% total lithics and

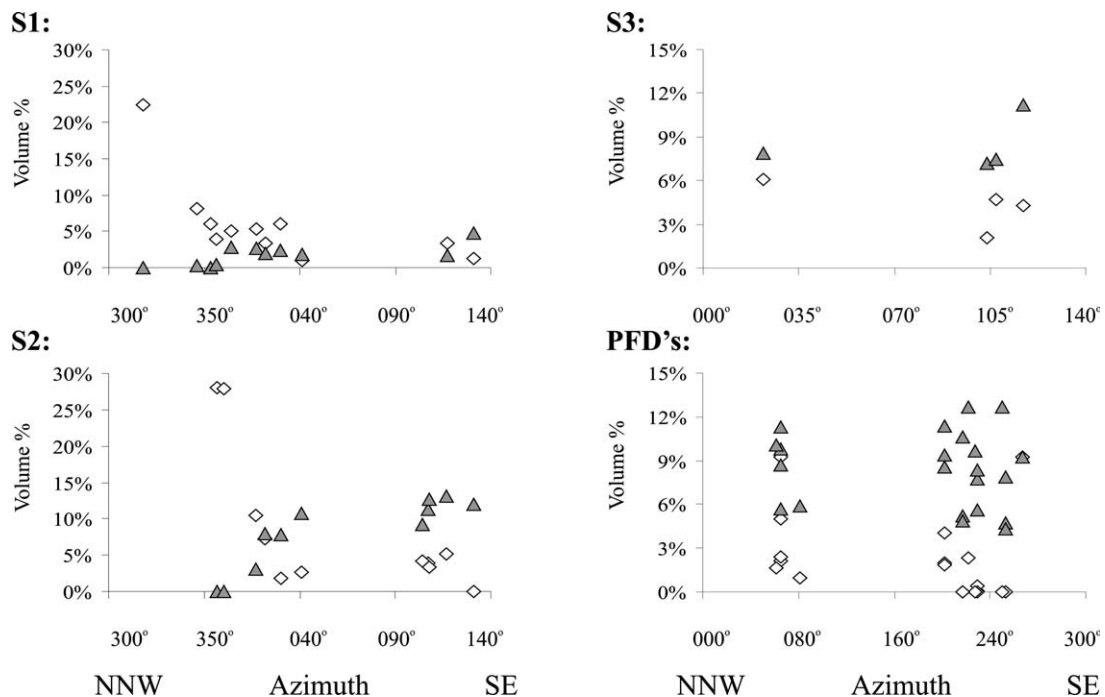


Fig. 3. Abundance of granitic clast lithics (GC, open diamonds) and Jala–Juanacata lithics (JJ, filled triangles) around Volcán Ceboruco from the S1, S2, S3 pyroclastic surge deposits and the Phase III PFDs, starting clockwise from the NNW sample locality (Loc. 11; see Fig. 1). All three surge deposits display systematic changes in GC and JJ abundance with proximity to either the north-flank vent or south-flank ring-vent, where deposits near the north-flank vent are enriched in GC and deposits near the south-flank ring-vent are enriched in JJ. This trend is no longer observed in the PFDs from Phase III (lower right), where deposits are equally enriched in JJ regardless of proximity to either vent. Phase III PFDs do, however, display a depletion trend in GC with increased proximity to the south-flank ring-vent that is consistent with the Phase II surge deposits.

is composed almost entirely of FV (86.1 vol%), with negligible amounts of JJ (<1 vol%) and GC (13.5 vol%).

5.2. Phase II deposits

Overall, S1 deposits are relatively lithic-rich, containing between 25 and 60 wt% total lithics (Table 1). In S1 deposits, the abundance of GC steadily increases with proximity to the north-flank vent, accounting for less than 2 vol% on the southeast flanks to 22.4 vol% NW of the single vent (Fig. 3). The opposite pattern is observed for JJ and FV abundances, where an increasing trend with proximity to the eastern caldera rim is observed. S1 samples on the east flanks contain 1.7–4.7 vol% JJ, whereas samples near the north-flank vent contain <0.4 vol%. Likewise, the proportion of FV steadily increases from 77.6 vol% NW of the north-flank single vent to 94 vol% on the south flanks. Isopach measurements from S1 occur in two distinct lobes, one to the northeast and one to the southeast (Fig. 1). This dispersal pattern is unique with respect to the dispersal direction of the Plinian fall deposits of the Jala Pumice.

Lithic fragments in P2 are similar throughout the dispersal area, and match those in other Plinian fall layers of the Jala Pumice. Some P2 deposits contain up to 75 wt% total lithics with the most lithic-rich regions existing at the base and top horizons (Table 1; Fig. 2). At the base of P2, FV account for 89.6–93.8 vol%, with minor amounts of GC (4.8–5.9 vol%) and JJ (1.1–4.5 vol%), marking a decrease in GC lithics compared with P1. In the middle horizons of P2, FV continues to account for the majority of lithic types (84.8–91.3 vol%), with a slight increase in GC (6.6–12.9 vol%) and decrease in JJ (2.1–2.8 vol%). The top of P2 resembles the proportions observed at the base, with 94.3–95.8 vol% FV, 3.7–5.4 vol% GC, and 0.3–0.5 vol% JJ.

Overall, S2 contains an average of 37 wt% total lithics, with one deposit containing as much as 67.7 wt% lithics (Table 1; Fig. 2). Isopach measurements from S2 indicate that this deposit was broadly dispersed to the northeast of Ceboruco (Fig. 1), and does not occur in two distinct lobes

as observed in S1. In the S2 deposits, the proportion of FV increases from 71.9 vol% at sites located to the NNW of the north-flank single vent, and to 81.7–88.0 vol% on the east and south flanks (Fig. 3). The abundance of GC steadily increases with proximity to the north-flank vent, accounting for <1–5.2 vol% on the southeast

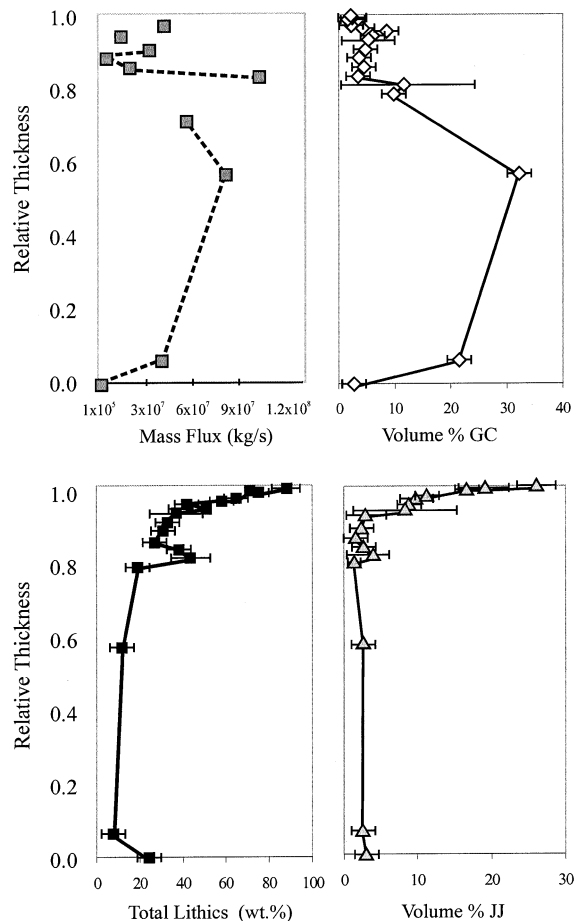


Fig. 4. Mass flux calculations for horizons within the Jala Pumice Plinian fall layers P0, P1, P2, P3, and P4 (from Gardner and Tait, 2000) compared to GC abundance (top) and total accidental lithic content (wt%) compared to JJ abundance (base). Note that GC abundance mirrors that of mass flux, indicating that deep-origin lithics were preferentially eroded with increasing mass flux. The abundance of JJ, however, reflects the total lithic content, suggesting that shallow-origin lithics were preferentially eroded with continued caldera collapse.

flanks to 27.9–28.1 vol% at sites located NNW of the single vent. For JJ, the opposite pattern is observed, increasing with proximity to the eastern caldera rim. S2 samples on the east flanks contain 12.0–13.1 vol% JJ, whereas samples near the north-flank vent contain < 3.1 vol%.

The P3/4 fall layer contains between 26.45 and 90.4 wt% total lithics, with the base and top horizons richest in lithics. The proportion of lithic components from the P3/4 fall layer shows a progressive increase in JJ as a function of decreasing FV and GC. The abundance of FV and GC (88.0–91.1 vol% and 3.4–6.3 vol%, respectively) decreases from base to top (85.9–90.4 vol% and 3.4–5.6 vol%, respectively). The proportion of JJ, steadily increases from 5.5 vol% at the base to 9.4 vol% at the top.

S3, located only on the southeastern flanks of Ceboruco, contains a similar proportion of FV, GC, and JJ compared with the S2 deposits found in the same region. FV account for 84.5–90.7 vol%, GC account for 2.1–6.1 vol%, and JJ account for 7.2–11.2 vol%. Overall, S3 contains between 34.3 and 67.1 wt% total lithics (Fig. 2). Isopach measurements from S3 are thickest to the southeast of Ceboruco (Fig. 1). The axis of this dispersal pattern points to the southeast flank of Ceboruco, rather than the north-flank vent.

5.3. Phase III deposits

Although the North-Flank and Marquesado PFDs are equally lithic-rich, containing an average of 60 wt% total lithics, the proportions of GC and JJ lithic types continue to vary with proximity to the north vent (Fig. 3). Phase III pyroclastic deposits located adjacent to the northern vent (North-Flank PFDs) contain 81.5–93.1 vol% FV, 5.7–11.3 vol% JJ, and 1.0–9.2 vol% GC. Deposits found to the south (Marquesado PFDs) contain 85.0–95.7 vol% FV, 4.3–12.7 vol% JJ, and < 0.4–2.3 vol% GC.

Phase III lithic falls (L1, L2, and L3) contain up to 90 wt% total lithics, and are rich in JJ (6.7–18.4 vol%) and FV (81.1–93.3 vol%), while containing few GC (0.0–1.8 vol%). L1, L2, and L3 have only been recognized within 3 km from Ceboruco, and are thickest on the eastern flanks.

6. Discussion and conclusions

Many caldera-forming eruptions apparently experience a transition at some point during the eruption from a single-vent Plinian phase to a subsidence-related ring-vent phase (Bacon, 1983; Lipman, 1984; Heiken and McCoy, 1984; Druitt and Sparks, 1984; Hildreth and Mahood, 1986; Rosi et al., 2001). The AD ~1000 eruption of Volcán Ceboruco also followed this pattern, as indicated by mass flux and total lithic content arguments (Fig. 4) (Gardner and Tait, 2000), shifting isopachs from interbedded Plinian fall and pyroclastic surge layers (Browne, 2001), and lithic fragment population data that allow for the recognition of a shift in eruptive style from single-vent to multiple vents that began at the start of Phase II.

The lithic fragments of the Phase I deposits are dominantly vent-derived or of deep-origin. The eruption began from a single vent on the north flank with the narrow dispersal of P0, a thin, fine-grained deposit composed of > 90 vol% vent-derived lithics. P1 was erupted next as a well-sorted, coarse-grained Plinian fall deposit that accounts for > 60 vol% of the Jala Pumice. Although P1 contains fewer total lithics compared with any other layer (< 15 wt%), it contains the largest proportion of deep-origin granitic lithics in the Jala Pumice. The end of Phase I is marked by the rapid normal grading at the top of P1, suggesting that the eruption experienced an abrupt decrease in intensity. We interpret this pattern to signify the beginning and end of the single-vent phase of this eruption. It is intuitive that initial vent-clearing activity resulted in a dominance of vent-derived lithics in the P0 horizon. Once a stable Plinian column was established during the deposition of P1, however, the efficient removal of magma from the AD ~1000 magma chamber to the surface resulted in a shift in lithic erosion from the vent to include erosion of lithics from depths closer to the magma chamber as well.

The base of the Phase II deposits is marked by a thin, fine-grained, lithic-rich level immediately above P1 and below S1, that is composed of > 95 vol% vent-derived lithics, similar to that of

P0. Above that, Phase II deposits are distinct from Phase I, in that they are alternating beds of lithic-rich Plinian fall and pyroclastic surge deposits that exhibit a steadily increasing abundance of vent-derived and intermediate-depth lithics. Deposits at the top of Phase II contain approximately 90 vol% vent-derived lithics, and subequal proportions of lithics of intermediate and deep origin in comparison with deposits at the base of Phase II that are composed of as much as 25 vol% deep-origin lithics. We interpret this to suggest that Phase II began similarly to Phase I with the narrow dispersal of a thin, fine-grained deposit composed almost entirely of vent-derived lithics. The subsequently erupted deposits, however, indicate that the predominant depth of lithic erosion decreased from Phase I to Phase II. Plinian fall deposits emplaced during Phase II contain a nearly constant population of vent-derived and deep-origin lithic fragments, whereas pyroclastic surges contain varying amounts of deep-origin granitic fragments or intermediate-depth lithics with increased proximity to the north or southeast flank, respectively.

Isopachs from pyroclastic surge deposits erupted during Phase II exhibit a dispersal pattern distinctly different compared with the Plinian fall layer isopachs. Whereas Plinian fall isopachs indicate an eruptive origin of the north-flank vent, isopachs from Phase II pyroclastic surge deposits indicate multiple vents. We argue that this transition from single to multiple vents coincided with the onset of caldera collapse. In addition, the north-flank and southeastern-flank vents appear to have been simultaneously active because the Phase II pyroclastic surge and Phase III flow deposits are interbedded with Phase II Plinian fall layers. Phase II surge deposit isopachs progressively shift from the northeastern dispersal direction, characteristic of Plinian fall deposits, to the southeast as the eruption continued. In addition, Phase II pyroclastic surge deposits contain a decreasing proportion of deep-origin lithics and an increasing proportion of vent-derived lithics and lithics from intermediate depths in a clockwise pattern from north to southeast. This trend is also observed in reverse, where the ratio of deep-origin lithics in pyroclastic deposits progres-

sively increases with increased proximity to the north-flank vent.

The change in predominant lithic erosion depth from deep to intermediate depths that was initiated during Phase II continued during Phase III as evidenced by the lithic population of the deposits. Deposits found at the top of the Jala Pumice stratigraphy contain more lithic fragments from intermediate depth, nearly 30 vol%, than any other layer and only minor amounts of deep-origin lithics. Lithic componentry of Phase III PFDs also indicates that the trend in lithic type with proximity to the north-flank or southeastern-flank vent that began in Phase II is maintained. Whereas deposits located to the south of Ceboruco are relatively enriched in vent-derived and intermediate-depth lithics, pyroclastic deposits to the north are enriched in deep-origin lithics. The absence of deep-origin lithics and steady decline in juvenile material (< 10 wt% pumice) from the uppermost Jala Pumice stratigraphy argues the fact that progressively less material from the AD ~1000 magma chamber reached the surface as the eruption closed.

A popular model used to explain caldera collapse is presented in [Druitt and Sparks \(1984\)](#). This model predicts that collapse occurs after a relatively small volume of magma has erupted along vertical or outward dipping faults. In this case, the vast majority of magma is forced out in response to the dense roof collapsing into a less dense magma reservoir. Quantitative component analysis studies of accidental lithics in pyroclastic deposits from large volume (> 10 km³) caldera eruptions, such as the Crater Lake and the Minoan deposits, suggest that lithics of the deepest origin were erupted during collapse ([Heiken and McCoy, 1984](#); [Suzuki-Kamata et al., 1993](#)). These observations were interpreted to agree with predictions from the model for caldera collapse presented by [Druitt and Sparks \(1984\)](#). In this study, the opposite is found, where lithics of shallow and intermediate depth origin are found in deposits erupted during collapse. Therefore, an alternative explanation should be considered.

We suggest that the AD ~1000 eruption of Ceboruco began from a vent located on the northern flank (Phase I; [Fig. 5](#)). Following a brief

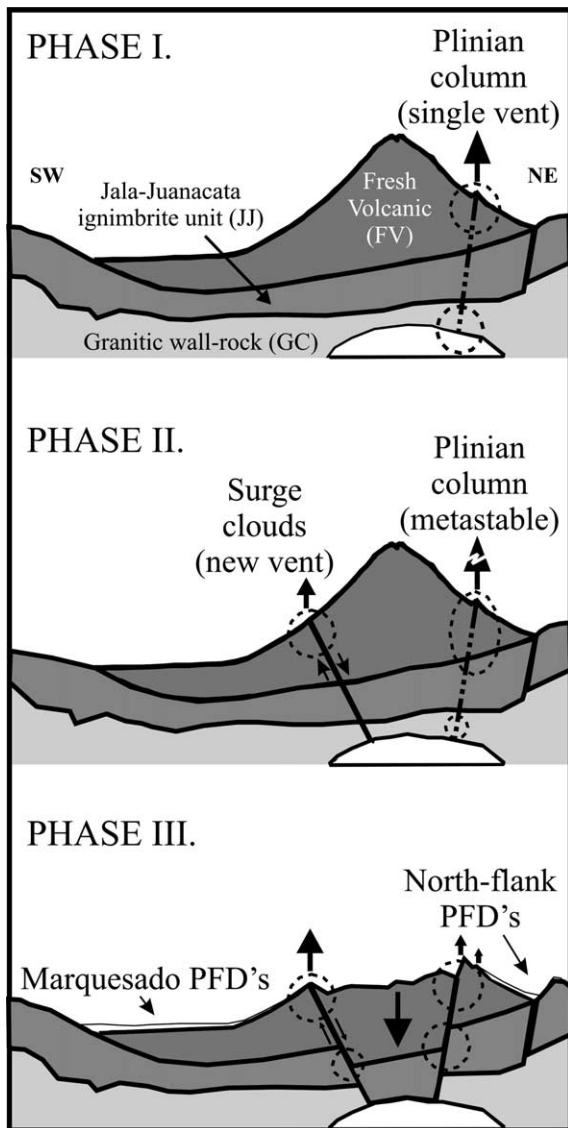


Fig. 5. Schematic diagram illustrating sequence of the AD ~1000 Jala Pumice eruption and caldera collapse. Subsurface stratigraphy inferred by Thorpe and Francis (1975), Nelson (1980), and Ferrari et al. (1999). Dashed circles represent regions of accidental lithic erosion for each phase of the eruption indicated from component analysis. Note that collapse is interpreted to occur along inward dipping faults which act to close the conduit, subsequently shutting off the eruption.

pause in the activity, the eruption was reinitiated as vent-clearing activity with the emplacement of a thin, fine-grained fall layer immediately atop P1 (Phase II) from the north-flank immediately followed by S1 from both the north-flank vent as well as another vent on the southeast flank. The initiation of a multiple vent on the southeast flank symbolizes the onset of caldera collapse (Fig. 5). We suggest that collapse occurred via the fracturing and subsequent failure of the overlying roof along inward dipping faults rather than along vertical or outwardly dipping faults, as evidenced by the fact that the volume of magma that erupted prior to collapse is considerably more compared to that which was erupted during and after collapse, and that progressively less magma was erupted as collapse concluded. The failing and fracturing of rock was progressive rather than abrupt as evidenced by the gradual increase of lithics of shallow and intermediate depth being erupted through the stratigraphy. We speculate that a change in vent geometry probably accompanied collapse, which forced the erosion and entrainment of lithic material from deep (~6 km) to mid-depth (~1 km), subsequently sealing the conduit, and stopping the eruption (Fig. 5).

Acknowledgements

Jose Luis Macías, Alain Burgisser, and Luca Ferrari are gratefully acknowledged for their helpful suggestions and thought-provoking discussions. We would also like to thank Ricardo Saucedo and Jose Luis Arce for their gracious assistance and generous cooperation while in the field. Constructive and insightful suggestions offered by Claus Siebe and an anonymous reviewer certainly led to a much-improved manuscript. We would also like to thank Carrie Browne for her enthusiasm and support.

References

- Bacon, C.R., 1983. Eruptive history of Mount Mazama and Crater Lake Caldera, Cascade Range, USA. *J. Volcanol. Geotherm. Res.* 18, 57–115.

- Browne, B.L., 2001. Eruptive Stratigraphy and the Transport and Deposition of Pyroclastic Material from the Caldera-Forming Eruption of Volcán Ceboruco, Nayarit, Mexico. Unpubl. M.Sc. Thesis, University of Alaska, Fairbanks, AK.
- Carey, S., Sigurdsson, H., 1987. Temporal variations in column height and magma discharge rate during the 79 AD eruption of Vesuvius. *Geol. Soc. Am. Bull.* 99, 303–314.
- Demant, A., 1978. Características del eje neovolcanico trans-mexico y sus problemas de interpretacion. *Univ. Geol. Rev.* 2, 172–187.
- Druitt, T.H., Sparks, R.S.J., 1984. On the formation of calderas during ignimbrite eruptions. *Nature* 310, 679–681.
- Ferrari, L., Pasquaré, G., Venegas-Salgado, S., Romero-Rios, F., 2000. Geology of the western Mexican Volcanic Belt and adjacent Sierra Madre Occidental and Jalisco block. *Geol. Soc. Am. Spec. Pap.* 344, 65–83.
- Gardner, J.E., Tait, S., 2000. The caldera-forming eruption of Volcán Ceboruco, Mexico. *Bull. Volcanol.* 62, 20–33.
- Gunn, B., Mooser, F., 1971. Geochemistry of the volcanics of central Mexico. *Bull. Volcanol.* 62, 577–614.
- Heiken, G., McCoy, F., 1984. Caldera development during the Minoan eruption, Thira, Cyclades, Greece. *J. Geophys. Res.* 89, 8441–8462.
- Hildreth, W., 1977. The Magma Chamber of the Bishop Tuff; Gradients in Temperature, Pressure, and Composition. Unpubl. Ph.D. Thesis, University of California, Berkeley, CA.
- Hildreth, W., 1991. The timing of caldera collapse at Mount Katmai in response to magma withdrawal toward Novarupta. *Geophys. Res. Lett.* 18, 1541–1544.
- Hildreth, W., Mahood, G.A., 1986. Ring-fracture eruption of the Bishop Tuff. *Geol. Soc. Am. Bull.* 97, 396–403.
- Lipman, P., 1984. The roots of ash flow calderas in western North America: Windows into the tops of granitic batholiths. *J. Geophys. Res.* 89, 8801–8841.
- Nelson, S.A., 1980. Geology and petrology of Volcán Ceboruco, Nayarit, Mexico. *Geol. Soc. Am. Bull.* 91, 2290–2431.
- Newhall, C.G., Punongbayan, R.S. (Eds.), 1996. Fire and Mud: Eruptions and Lahars of Pinatubo volcano, Philippines. PHIVOLCS, Quezon City, and University of Washington Press, Seattle, WA.
- Ordoñez, E., 1897. Les volcans Colima et Ceboruco. *Mem. Soc. Sci., Antonio Alzate* 7, Mexico, 11, 329–333.
- Rampino, M., Self, S., 1982. Historic eruptions of Tambora (1815), Krakatoa (1883), and Agung (1963), their stratospheric aerosols and climactic impact. *Quat. Res.* 18, 127–143.
- Rosi, M., Paladio-Melosantos, M.L., Di Muro, A., and others, 2001. Fall vs flow activity during the 1991 climatic eruption of Pinatubo Volcano (Philippines). *Bull. Volcanol.* 62, 549–566.
- Scott, W.E., Hoblitt, R.P., Torres, R.C., Self, S., Martinez, M.L., Nillos, T., 1996. Pyroclastic flows of the June 15, 1991, climactic eruption of Mount Pinatubo. In: Newhall, C.G., Punongbayan, R.S. (Eds.), *Fire and Mud: Eruptions and Lahars of Mount Pinatubo, Philippines*. University of Washington Press, Seattle, WA, pp. 545–570.
- Sigurdsson, H., Carey, S., Cornell, W., Pescatore, T., 1985. The eruption of Vesuvius in A.D. 79. *Natl. Geogr. Res.* 1, 332–387.
- Smith, R.L., 1979. Ash-flow magmatism. *Geol. Soc. Am. Spec. Pap.* 180, 5–27.
- Smith, R.L., Bailey, R.A., 1968. Resurgent cauldrons. *Geol. Soc. Am.* 116, 613–662.
- Suzuki-Kamata, K., Kamata, H., Bacon, C.R., 1993. Evolution of the caldera-forming eruption at Crater Lake, Oregon, indicated by component analysis of lithic fragments. *J. Geophys. Res.* 98, 14059–14074.
- Thorpe, R.S., Francis, P.W., 1975. Volcán Ceboruco: A major composite volcano of the Mexican Volcanic Belt. *Bull. Volcanol.* 39, 201–213.
- Williams, H., 1941. Calderas and their origin. *Calif. Publ. Bull. Dep. Geol. Sci.* 25, 239–346.
- Wilson, C.J.N., Hildreth, W., 1997. The Bishop Tuff: New insights from eruptive stratigraphy. *J. Geol.* 105, 407–439.